Supplementary Materials

Efficient Photocatalytic Reactions of Cr(VI) Reduction, Ciprofloxacin and RhB Oxidation with Sn(II) Doped BiOBr

Ling Xu[a], Wen-qian Chen[a,c]*, Shu-qiang Ke[a], Min Zhu[a], Wen-hui Qiu[c,d], Ning Liu[e], Supawadee Namuangruk[f], Phornphimon Maitarad[g], Sarawoot Impeng[f], Liang Tang[a,b]*

[a] School of Environmental and Chemical Engineering, Shanghai University, Shanghai 200444, PR China

[b] Key Laboratory of Organic Compound Pollution Control Engineering, Ministry of Education, Shanghai 200444, PR China

[c] Shanghai Institute of Applied Radiation, Shanghai University, 20 Chengzhong Road, Shanghai 201800, PR China

[d] Guangdong Provincial Key Laboratory of Soil and Groundwater Pollution Control, School of Environmental Science and Engineering, Southern University of Science and Technology, Shenzhen 518055, PR China

[e] School of Environment and Architecture, University of Shanghai for Science and Technology, Shanghai 200093, PR China

[f] National Nanotechnology Center (NANOTEC), National Science and Technology Development Agency (NSTDA), Thailand

[g] Research Center of Nano Science and Technology, Shanghai University, Shanghai 200444, P. R. China

* Corresponding author. E-mail addresses: wenqianchen@shu.edu.cn (W. Q. Chen), tang1liang@shu.edu.cn (L. Tang)

Computational details

Spin-polarized periodic DFT calculations were carried out using the Vienna Ab Initio Simulation Package (VASP).[1] The generalized gradient approximation (GGA) with the PBE (Perdew−Burke−Ernzerhof) functional was used to calculate exchange-correlation energies.[2] The projector augmented wave method (PAW) was applied to describe the electron-ion interaction.[3] A kinetic energy cutoff for the plane-wave basis set was set at 520 eV. The D3 scheme of Grimme was used to account for the dispersion interactions.[4] For geometry optimization, the Brillouin zone integration was performed using Monkhorst-Pack (MP) scheme with 6 × 6 × 3 k-points.[5] Based on the optimized structures, the band structures were calculated along the special lines connecting the following high-symmetry points: G (0, 0, 0), X (0, 0.5, 0), Z (0, 0, 0.5), M (0.5, 0.5, 0), R (0, 0.5, 0.5), and A (0.5, 0.5, 0.5) in the k-space. Vesta program was used for visualization of molecular structures. Band structure results were analyzed by using p4vasp.

To demonstrate the effect of Sn^{2+} doping on the photocatalytic performance of BiOBr, we adopted the Bi-to-Sn molar ratio at 1:0, 3:1, and 1:1, to represent the prepared catalysts; BOB, S3-BOB and S5-BOB, respectively, in our experiment. In details, the 2 × 2 × 1 unit cell of BiOBr consisting of 8 atoms of Bi, O, and Br was employed for representing BOB catalyst. For the S3-BOB and S5-BOB catalysts, two and four Bi atoms were substituted by Sn atoms to model the 3:1 and 1:1 ratios of Bi:Sn, respectively. Subsequently, two and four Br atoms were removed to neutralize the system because the Bi, Sn, and Br have different oxidation state of +3, +2, and -1,

respectively. Since at 3:1 and 1:1 ratio there are many possible substitutions of Bi by Sn and removals of Br from the system, we first performed energy minimization to find the most stable structure. After that, only the most stable structure of Sn-doped BiOBr was performed for the band structure calculations, see Figure S9.

Table S1 BET specific surface area, pore volume and average pore diameter of BOB and S3-BOB.

Sample	**BET(m^2/g)[a]**	**Pore Volume(cc/g)[b]**	**Pore Diameter(nm)[c]**
BOB	23.478	0.08553	1.45724
S3-BOB	57.546	0.4299	2.98838

[a] BET specific surface.

[b] Total pore volume measured at P/P0=0.99.

[c] Average Pore Diameter of the sample.

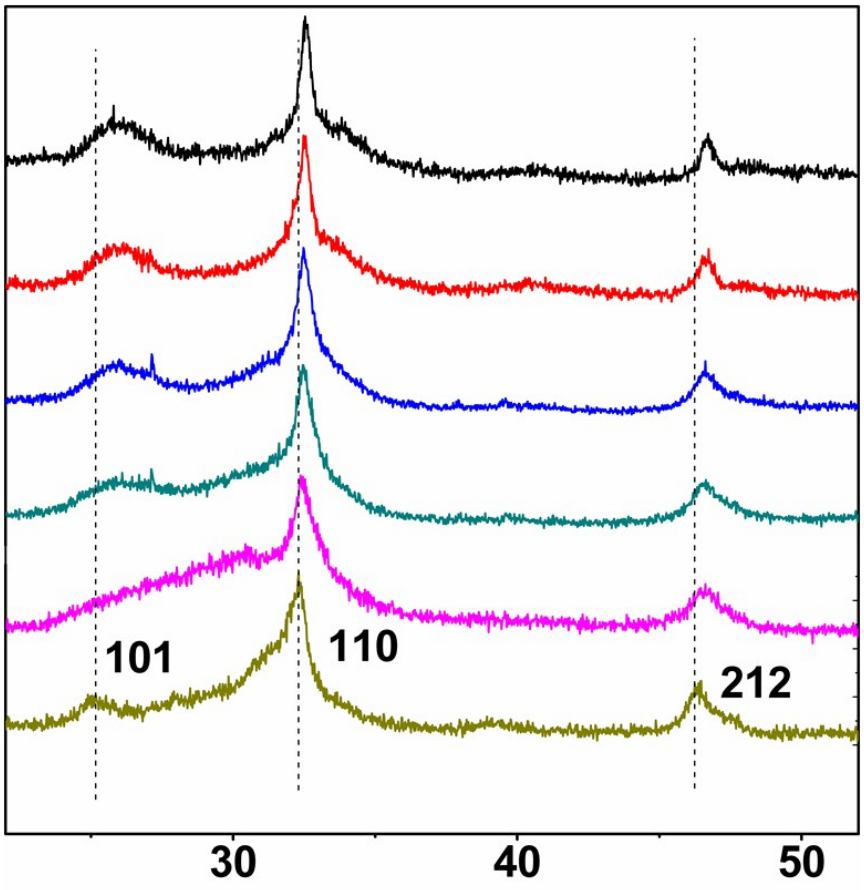

Figure S1. The Partial enlargement XRD patterns of BOB and S-BOB composites.

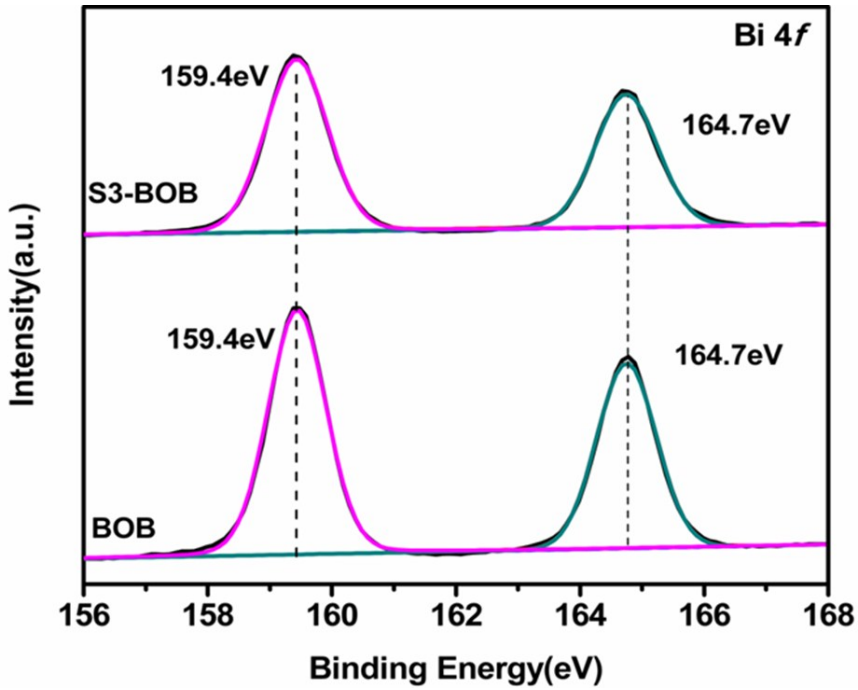

Figure S2. XPS spectra of Bi 4f in BOB and S3-BOB

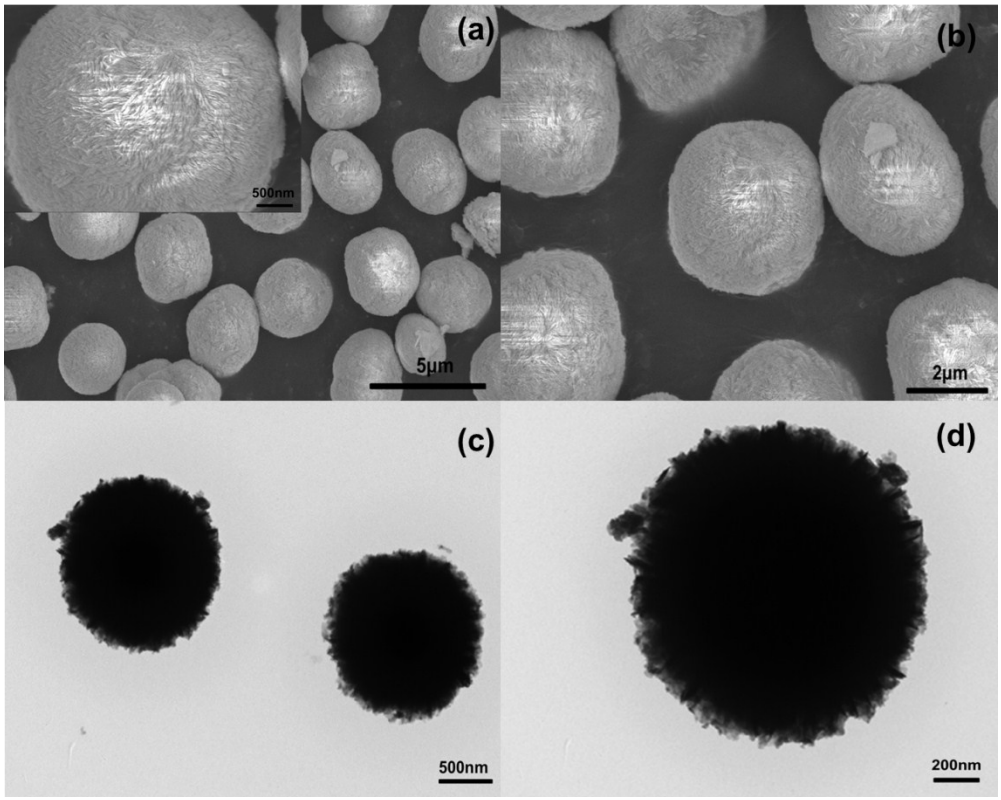

Figure S3. SEM images (a, b) and TEM images (c, d) of BOB

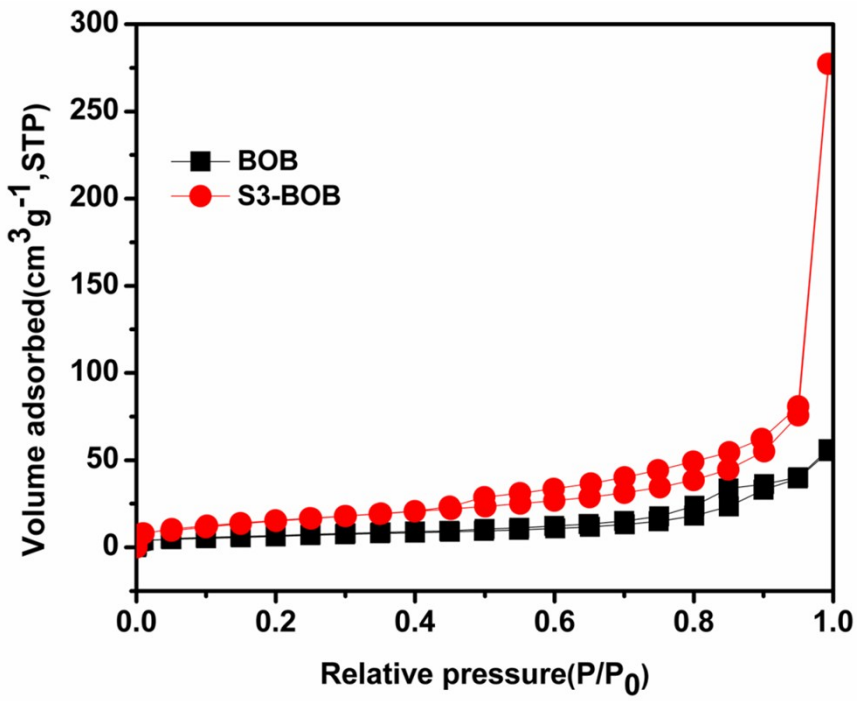

Figure S4. Nitrogen adsorption-desorption isotherm of BOB and S3-BOB.

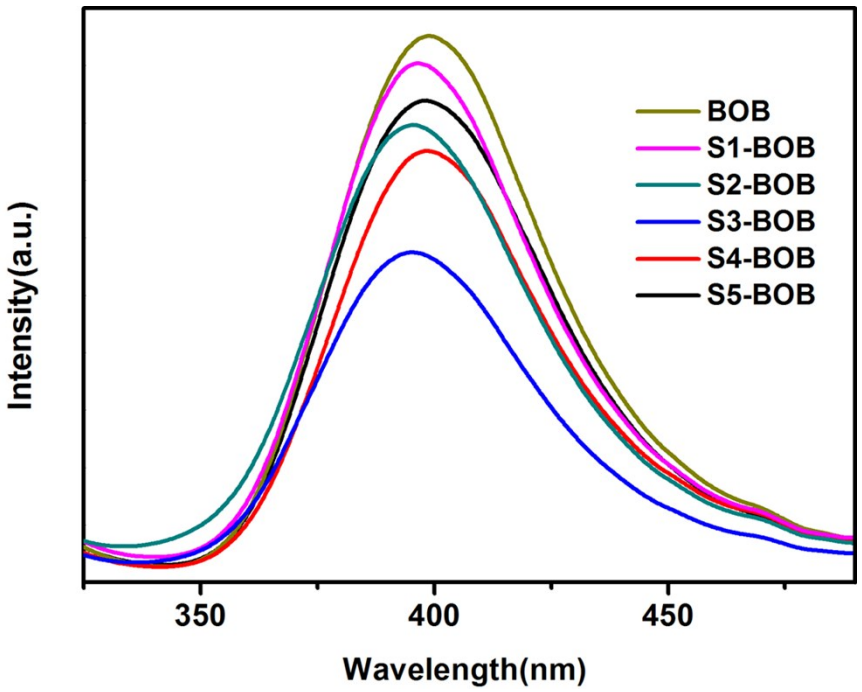

Figure S5. Photoluminescence (PL) spectra of BOB and S-BOB.

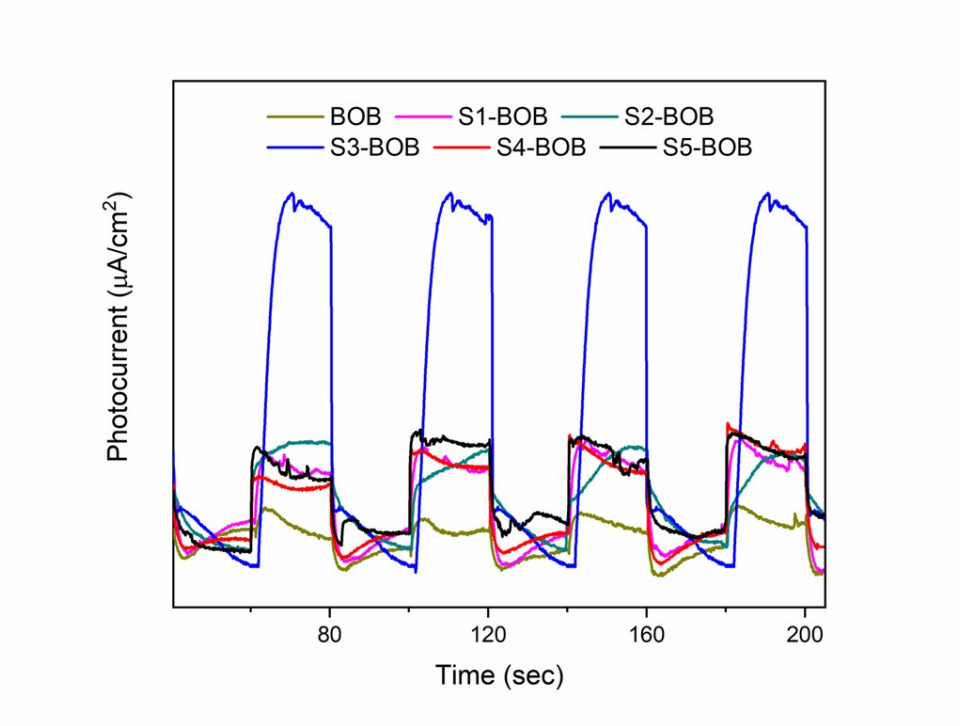

Figure S6. The photocurrent response of BOB and S-BOB.

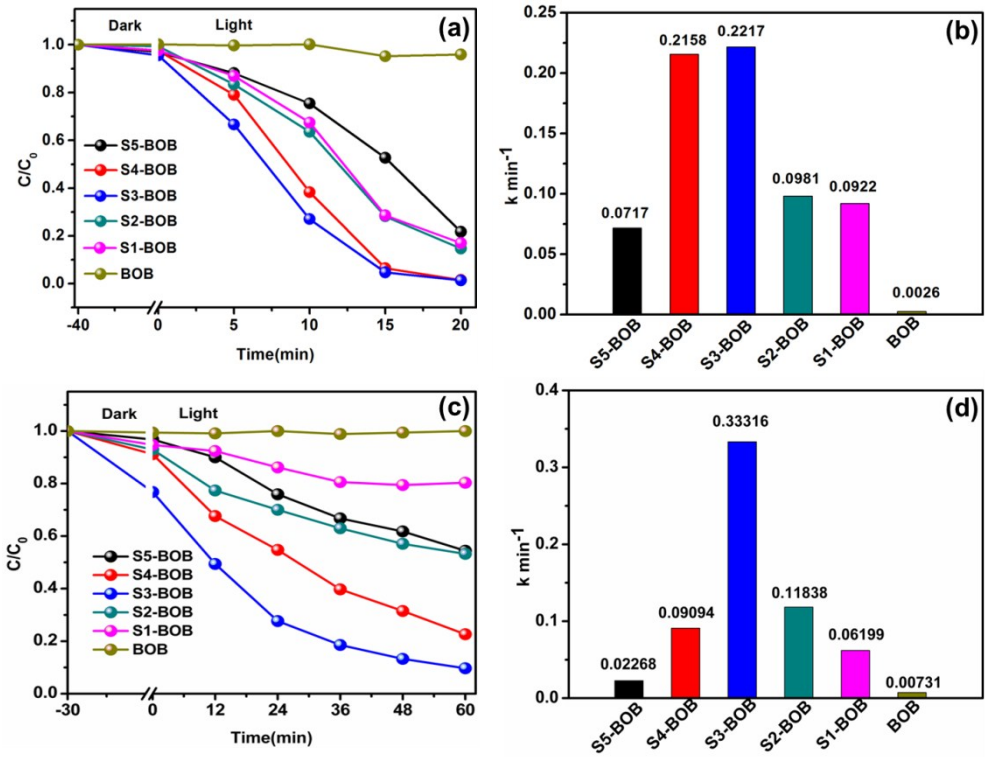

Figure S7. (a) Photocatalytic degradation curves of RhB. (b) The apparent reaction rate constants (k) of RhB. (c) Photocatalytic reduction curves of the Cr (VI). (d) The apparent reaction rate constants (k) of Cr (VI).

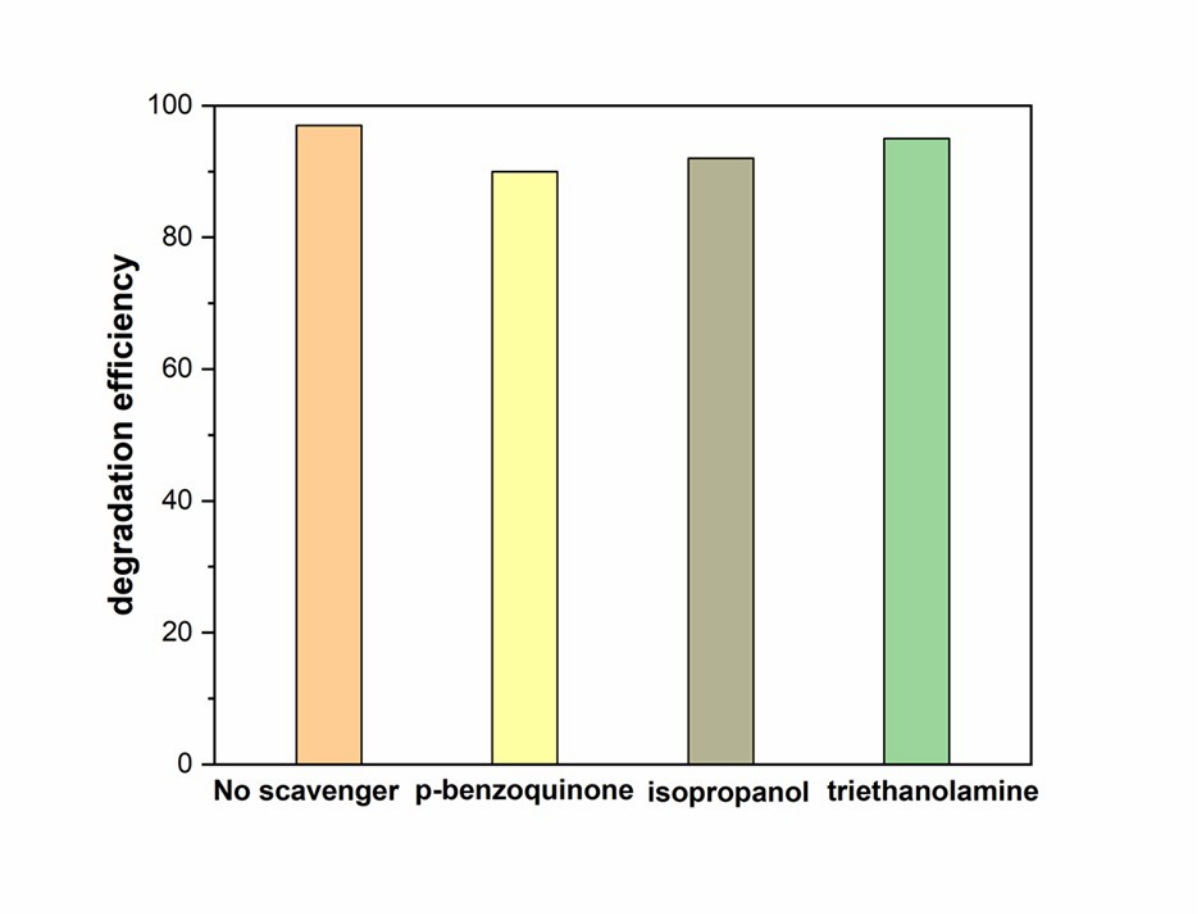

Figure S8. Effects of different scavengers on the Cr(VI) reduction with S3-BOB

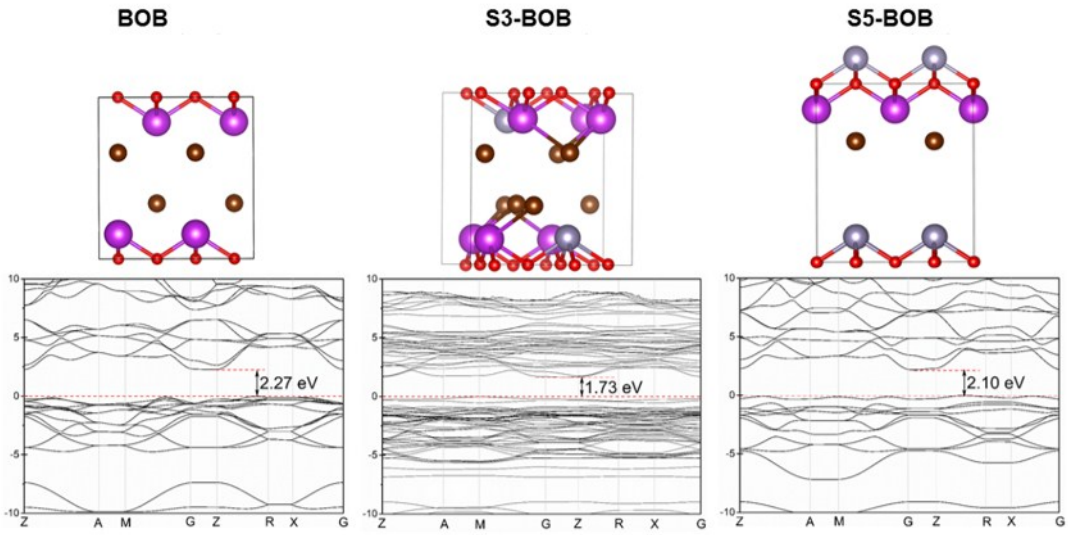

Figure S9. The most stable structures (upper) and band structures (below) of BOB, S3-BOB, and S-BOB.

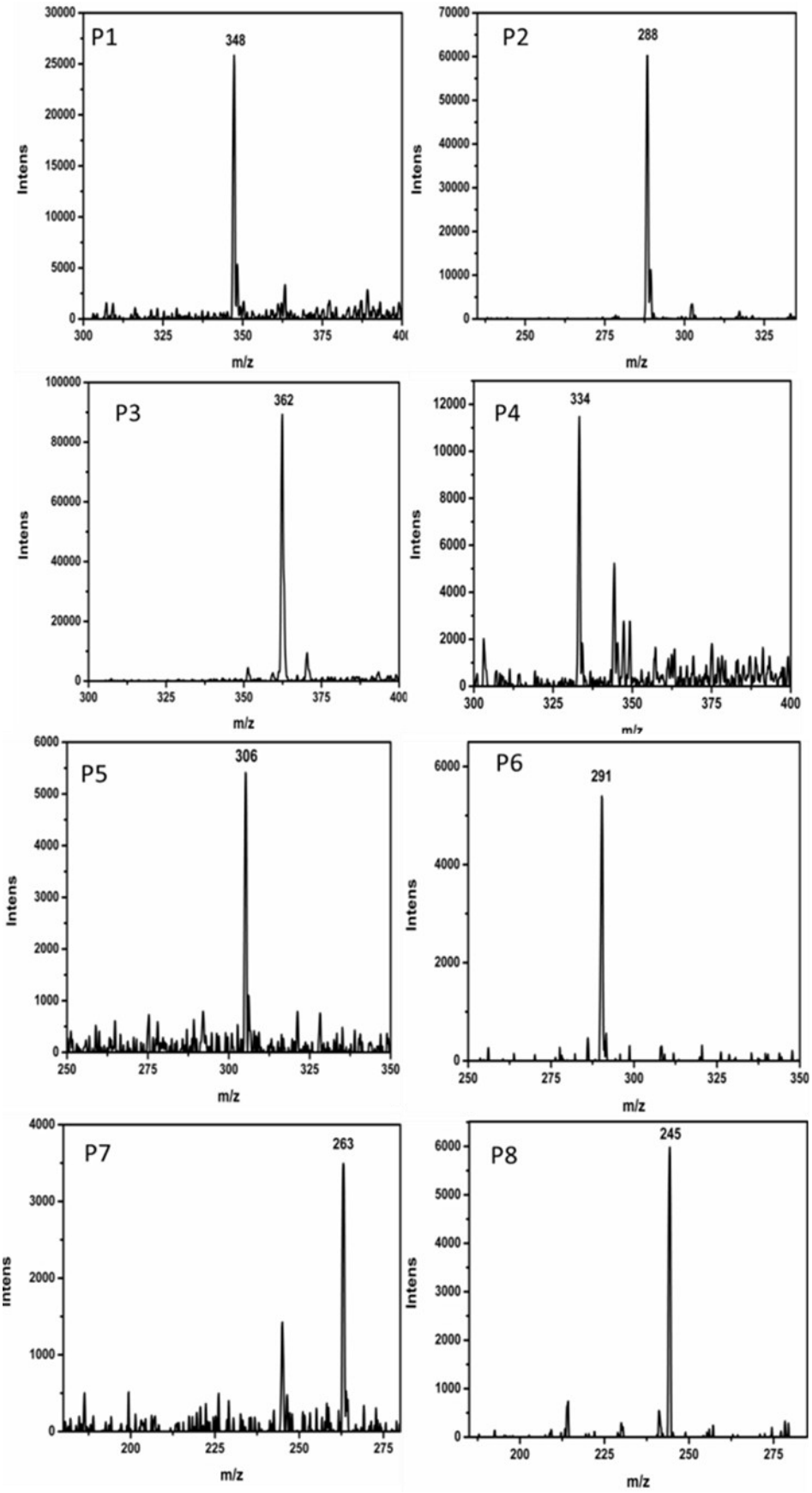

Figure S10. The mass spectrum of the main intermediate production.

References

1. Kresse, G.; Furthmüller, J., Efficient iterative schemes for ab initio total-energy calculations using a plane-wave basis set. *Physical Review B - Condensed Matter and Materials Physics* **1996,** *54* (16), 11169-11186.
2. Perdew, J. P.; Burke, K.; Ernzerhof, M., Generalized gradient approximation made simple. *Physical Review Letters* **1996,** *77* (18), 3865-3868.
3. Kresse, G., From ultrasoft pseudopotentials to the projector augmented-wave method. *Physical Review B - Condensed Matter and Materials Physics* **1999,** *59* (3), 1758-1775.
4. Grimme, S.; Antony, J.; Ehrlich, S.; Krieg, H., A consistent and accurate ab initio parametrization of density functional dispersion correction (DFT-D) for the 94 elements H-Pu. *The Journal of Chemical Physics* **2010,** *132* (15), 154104.
5. Monkhorst, H. J.; Pack, J. D., Special points for Brillouin-zone integrations. *Physical Review B* **1976,** *13* (12), 5188-5192.